Paper pa02-062
Submitted to the 28th International Conference on High Energy Physics
ICHEP'96, Warsaw, Poland, July 1996

Measurements of Jet Production and Energy Flow in Diffractive *ep* Interactions at HERA

H1 Collaboration

Abstract

The properties of the hadronic final state X in diffractive ep interactions are presented using data collected by the H1 experiment at HERA. The data were taken during 1994 and correspond to $\sim 2\,\mathrm{pb}^{-1}$. Measurements of the energy flow $\frac{1}{N}\frac{\mathrm{d}E}{\mathrm{d}\eta^*}$ are made in the γ^*-pomeron ($I\!\!P$) centre–of–mass system for different regions of M_X, the mass of system X. For all values of M_X the data exhibit a significant excess of energy production in the central ($\eta^* \sim 0$) region over that expected for a quark dominated process. Cross sections for the diffractive production of di-jets of invariant mass squared $\hat{s}$ are evaluated differentially as functions of x_γ and z in the laboratory frame for $Q^2 < 4$ GeV^2 with x_γ being the momentum fraction of the parton in the γ entering the hard subprocess and (z) the momentum fraction of the 2–jets from the hard subprocess at the hadron level. Cross sections are also presented as functions of P_T^2 and $\xi_{I\!\!P}$ in the γ^*-$I\!\!P$ centre–of–mass systems for $Q^2 > 4$ GeV^2. The distribution in ξ is demonstrated to be sensitive to the gluon distribution in the diffractive exchange. The data for both di-jet production and energy flow are well described by Monte Carlo predictions based on a partonic model of $eI\!\!P$ interactions in which the parton densities are derived from a QCD analysis of the diffractive structure function $F_2^{D(3)}$. In this ansatz the gluons are concentrated near $x_{g/I\!\!P} = 1$ at $Q^2 \sim Q_0^2 = 2.5$ GeV^2 and carry most of the momentum of the diffractive exchange.

Introduction

The measurements of energy-flow and inclusive charged particle spectra are sensitive tests of the partonic nature of the diffractive interaction. Measurements of the inclusive diffractive structure function $F_2^{D(3)}$ and the subsequent QCD analysis employing DGLAP evolution [1] yields a solution which tends towards a "leading" gluon.

In this paper the energy-flows and charged hadron distributions are analysed in the virtual-photon pomeron centre-of-mass system ($\gamma^* I\!P$ cms), which corresponds to the centre-of-mass of the diffractively produced hadronic final state with invariant mass M_X.

The invariant mass, M_X, of the hadronic system is defined by:

$$M_X^2 = \left(\sum_{had} p^\mu \right)^2$$

where the sum runs over all particles 4-momenta (p^μ) observed in the detector excluding the scattered electron. The fraction of the initial proton momentum carried by the exchanged color neutral particle, the pomeron $I\!P$, is then calculated using

$$x_{I\!P} = \frac{q.I\!P}{P.I\!P} \approx \frac{Q^2 + M_X^2}{Q^2 + W^2} \tag{1}$$

where W is the invariant mass of the $\gamma^* p$ system, q^μ the 4-momentum of the virtual photon, and P^μ of the 4-momentum of the incident proton

Measurements are made of energy flows in various M_X bins and of the inclusive charged track distributions in the kinematic region defined by $M_X > 3\,\mathrm{GeV}$, $7.5 < Q^2 < 100\,\mathrm{GeV}^2$, $0.05 < y < 0.6$, $x_{I\!P} < 0.025$. The data are compared with Monte-Carlo models based on the Ingelman-Schlein model [5] of deep-inelastic electron-pomeron scattering in which the parton densities have been determined from a QCD fit to $F_2^{D(3)}$. The charged particle spectra in X-Feynman (x_F) and p_T^{*2} are also compared with deep-inelastic electron-proton scattering (DIS) data for which $W \approx M_X$.

Measurements of $< p_T^{*2} >$ as a function of x_F have been found, from fixed target DIS experiments, to be very sensitive to higher order QCD effects. Further, details of the p_T^{*2} spectrum are also sensitive to non-perturbative fragmentation effects.

Measurements are also presented of the photoproduction di–jet cross section as a function of p_T^{*2} and x_γ, where x_γ is the momentum fraction of the parton in the photon.

For the high Q^2 sample we present the cross section as a function of p_T^2 and of the momentum fraction $\xi_{I\!P}$ carried by a parton participating in the hard subprocess:

$$\xi_{I\!P} = \frac{x}{x_{I\!P}}(1 + \frac{\hat{s}}{Q^2}) \tag{2}$$

where $\hat{s}$ is the invariant mass squared of the 2–jet system.

The Hadronic Final State

The hadronic final state is a sensitive test of the partonic structure of the pomeron. If the pomeron is believed to be a quark dominated object then this restricts the amount of transverse energy flow. For a simple quark dominated pomeron the "struck" quark and the "remnant" will be aligned along the $\gamma^* I\!P$ axis. The only contributions to the transverse momentum which would arise from the intrinsic transverse momentum (k_T) of the quark and the remnant. There is also a contribution from the fragmentation process. Both these contributions however produce relatively small amounts of transverse momentum.

However if the pomeron is a gluon dominated object then, from the boson-gluon fusion process (BGF), the quark anti-quark pair from the hard subprocess do not have to be aligned along the $\gamma^* I\!P$ axis. This then leads to high p_T di–jet final states in leading order. In higher order, wide angle soft gluon emission will also contribute to the energy flow in the central region of pseudo–rapidity and to $< p_T^{*2} >$.

In diffraction the relevant mass scale for the hadronic final state is M_X. Therefore it is logical to define x_F as

$$x_F = \frac{2p_z^*}{M_X} \tag{3}$$

where p_z^* is the longitudinal momentum component of the charged particle in the $\gamma^* I\!P$ cms. For this analysis the γ^* points in the direction of the positive z-axis.

Di–Jets

Diffractive di-jet production is sensitive to the structure of the pomeron. If the pomeron is similar to a particle consisting of quarks and gluons, then diffractive di-jet production at high Q^2 can originate from BGF

In photoproduction there are BGF and QCD-Compton contributions from direct photon interactions, and contributions from purely partonic hard interactions from resolved photons. From a measurement of $F_2^{D(3)}$ the quark densities in the $I\!P$ have been extracted and subsequently the contribution from QCD-Compton [1]. Hence the measurement of diffractive di-jet production is sensitive to the gluon density in the $I\!P$.

However the origin of the $I\!P$ is not clear. It is conceivable that the pomeron could be a two gluon state where the probability of finding a pomeron in the proton is given by the gluon density of the proton squared $[xg(x)]^2$. The two gluons can couple directly to a quark-antiquark pair, producing two high p_T jets and no pomeron remnant. This has been calculated for high Q^2 di–jet production by Lotter, Bartels, Wuesthoff and Diehl [6].

Event Selection

The data were collected in the 1994 running period of the H1 [4] detector at the HERA ep collider, operating with 27.5 GeV positrons colliding with 820 GeV protons. For the high Q^2 sample the events are triggered by requiring a minimum energy deposit in the backward electro-magnetic calorimeter (BEMC) ($E_{e'} \geq 4\,\mathrm{GeV}$). The data are then subject to the following selection. The cluster of energy in the BEMC is required to be greater 12 GeV and to be within the angular range $156° < \theta < 173°$ with respect to the proton beam direction . The energy deposit must also be associated with a hit in the backward proportional chamber (BPC) which is immediately in front of the BEMC.

Further kinematic constraints are $0.05 < y < 0.6$, $7.5 < Q^2 < 100\,\mathrm{GeV}^2$. For the di-jet analysis the kinematic constraints are $0.1 < y < 0.7$, $7.5 < Q^2 < 80\,\mathrm{GeV}^2$.

In the low Q^2 sample (photoproduction) the events are triggered by a signal in the small angle electron tagger, which restricts the kinematic region to $0.25 < y < 0.7$ and $10^{-8} < Q^2 < 0.01\,\mathrm{GeV}^2$.

Diffractive events are identified by the absence of energy in the forward region of H1. The events are rejected if they have more than 7.5 GeV in the plug calorimeter, more than one pair of hits in the first half of the forward muon detector, or any hits in the first three layers of the proton remnant tagger [2]. The pseudo-rapidity of the most forward cluster with more than 400 MeV, η_{max}, must be less than 3.0 for the energy-flow analysis and 3.2 for the di-jet analysis. The kinematic ranges also include the requirement $x_{I\!P}$ must be less than 0.025 for the energy-flow analysis or $x_{I\!P} < 0.05$ for the di-jet analysis.

The diffractively produced forward system Y is not detected. It is therefore not possible to distinguish a elastically scattered proton from one in which the proton dissociates into a low mass state. The cross section is quoted for the range $M_Y < 1.6\,\mathrm{GeV}$, where M_Y is the mass of the diffractively scattered proton remnant system.

For the energy flow analysis all calorimeter clusters within the rapidity gap are boosted to the $\gamma^* I\!P$ cms. The $\gamma^* I\!P$ cms is defined by reconstructing $x_{I\!P} = ((E + p_z)/2E_p)$. The energy and momentum correspond to the complete final state system including the electron. To reconstruct the complete cms vector (V^μ) information from the scattered electron is used such that $V^\mu = x_{I\!P} p^0 + q^\mu$, where p^0 corresponds to the energy of the proton in the HERA frame.

For the charged particle distributions, only tracks are used which are reconstructed in the central tracker (CJC) and which are fitted to the ep interaction vertex. Further more the range in pseudo-rapidity of the tracks is restricted to $-1.51 < \eta_{lab} < 1.64$ also the maximum transverse momentum of the track, p_{TMAX} is restricted to be less than 10 GeV so as to exclude badly measured tracks. The particles are then boosted to the $\gamma^* I\!P$ cms.

The jet finding is performed by applying a cone algorithm after boosting the respective objects into the $\gamma^* I\!P$ cms. The objects used in the cone algorithm are a combination of tracks measured in CJC and calorimeter clusters, where clusters associated to tracks are masked for tracks with momentum $p < 10\,\mathrm{GeV}$. In all other cases the energy and momentum of the clusters are used. The cone radius $\Delta R = 1$was chosen to be $\Delta R = \sqrt{\Delta\eta^2 + \Delta\Phi^2}$ where $\Delta\eta$ and $\Delta\Phi$ are the half widths in pseudo-rapidity and azimuthal angle respectively. In the $\gamma^* I\!P$ cms two jets with a transverse momentum $p_T^* > 5\,\mathrm{GeV}$ are required to have been found . Each jet is then subject to further restrictions. It must be within the geometrical acceptance of the detector and the the kinematic limits $0.1 < y < 0.7$, $x_{I\!P} < 0.05$, $7.5 < Q^2 < 80\,\mathrm{GeV}^2$, $M_Y < 1.6\,\mathrm{GeV}$.

Monte Carlo Models and Acceptance Corrections

To correct the various distributions the Monte Carlo event generator RAPGAP2.02 [7] was used. This is a perturbative model based upon diffractive hard scattering in $e^\pm - I\!P$ collisions with a partonic substructure assigned to the $I\!P$. In addition to the leading order $\mathcal{O}(\alpha)$ quark parton model diagram ($eq \to q$), Boson–gluon fusion ($eg \to q\bar{q}$) and

QCD–Compton ($eq \rightarrow qg$) processes are generated according to the order O($\alpha\alpha_s$) matrix elements. A $\hat{p}$ cut of $\hat{p} > 2$ GeV was introduced to avoid divergences of the matrix elements for massless quarks (RAPGAP ME+PS, where ME includes order α_s matrix elements and PS includes initial and final state parton showering).

Parton number density functions for the pomeron were taken from a leading order DGLAP [1] QCD analysis of the measured structure function $F_2^{D(3)}$ [2], and a simple factorisable $x_{I\!P}$ dependence equivalent to that of the $F_2^{D(3)}$ averaged over β was assumed.

The kinematic distributions and the overall features of the hadronic final state are well described by RAPGAP2.02. This simulation was then used to correct for the finite acceptance and resolution of the H1 apparatus such that cross sections are quoted at the hadron level.

The correlations of the jet rapidities η in the laboratory frame with y and $x_{I\!P}$ for a sample of Monte Carlo di-jet events simulated with the RAPGAP2.02 event generator [7] are shown in Fig. 1. It can be seen that by restricting the analysis to the kinematic region $x_{I\!P} < 0.05$ and $0.1 < y < 0.7$ then a cross section defined purely in terms of Lorenz invariant quantities may be evaluated from di-jet events which are fully contained in the H1 detector.

For the low Q^2 sample the Monte Carlo Generator POMPYT [8] was used with hard gluon or quark densities in the pomeron $\sim z(1-z)$ or a soft gluon density $\sim (1-z)^5$ where z is the momentum fraction $x_{i/I\!P}$ of the pomeron carried by the parton entering the hard interaction . A slightly different pomeron flux parametrisation is used. However this gives the same results as the one used in RAPGAP within the kinematic limits used.

Systematic Errors

In the evaluation of the systematic uncertainties on the corrected distributions the following sources of errors were considered:

- Uncertainties in the overall calibration of the liquid Argon calorimeter (LAr) by $\pm 4\%$.
- Uncertainties in the BEMC response for hadronic energy of $\pm 20\%$.
- Uncertainties in the measurement of the scattered positron. The energy scale uncertainty is varied by $\pm 1.6\%$, and the electron polar angle measurement by $\pm 2 mrad$.
- Uncertainties in the $x_{I\!P}$ dependence in the Monte Carlo.
- Uncertainties in the β dependence in the Monte Carlo.

The uncertainty arising from model dependence used to correct the data is studied. The systematic error is quoted as 100% the difference between the two different fragmentation schemes, one given by leading log parton showers, the other by the colour dipole model (CDM). The quoted error is $\pm 5\%$. For the energy flow analysis no single error dominates, except for $\eta^* > 1$ where the BEMC hadronic energy scale leads to an error of up to $\sim 10\%$.

For the charged particle analysis a further systematic error was introduced to account for the extrapolation to unseen momentum regions, this was achieved by varying the track selection. Tracks were selected to satisfy the following criteria, $-1.31 < \eta_{lab} < 1.31$, the number of hits on the track was required to be greater than 10 and the radial track length was required to be greater than 15 cm. This contributed a systematic error of $\pm 5\%$.

For the jets analysis the following further systematic errors were considered.

- As tracks and clusters are used as objects in the cone algorithm there is an uncertainty of $\pm 3\%$ in the track momentum scale.
- Uncertainty in the luminosity of $\pm 1.5\%$
- Uncertainties in the event selection efficiency leading to an error of 10%.
- Uncertainty in the photoproduction contamination of $\pm 50\%$.
- Uncertainty in the contamination arising from high $x_{I\!P}$ events (i.e. Normal deep-inelastic scattering) of $\pm 50\%$.
- Uncertainty on the noise contribution in the plug detector $(17. \pm 8)\%$).
- Uncertainty in the size of the radiative corrections giving rise to an error of 5%.
- Uncertainty on the proton dissociation contribution $(5. \pm 2.5)\%$.

Results

Energy Flow and Inclusive Charged Particle Distributions

Fully corrected energy flows in various M_X bins in the $\gamma^* I\!P$ cms are shown in fig. 2. Compared with the data are predictions from RAPGAP in which the parton densities were assumed to be only quarks at a starting scale of $Q_0^2 = 2.5\,\mathrm{GeV}^2$. Also compared is RAPGAP CDM which has parton densities obtained from a DGLAP fit to $F_2^{D(3)}$. It can be seen that the quark Monte Carlo fails by a substantial amount to account for the observed energy flow in the central pseudo-rapidity region, $\eta^* \approx 0$. The data is seen to be described well by a model that has the full QCD cascade implemented (RAPGAP + CDM).

The p_T^{*2} distribution is shown in fig. 3. The data at an average M_X of 10 GeV is compared with E.M.C. data at slightly higher centre-of-mass energies of $< W >= 14$ GeV and with RAPGAP2.02. It can be seen that there is a substantial tail in the p_T^{*2} distribution, suggesting a significant fraction of high p_T hard subprocess.

The p_T^{*2} dependence is reproduced by the RAPGAP-CDM model. The RAPGAP quark model however fails to describe the tail of the distribution.

The x_F distribution is shown in fig. 4. Again the data is compared with the E.M.C. result and a prediction from RAPGAP. It can be seen that the data fall off with increasing magnitude of x_F. One striking feature of the data is that the distribution is approximately symmetric about $x_F = 0$. This suggests that the forward and backward hemispheres have similar properties. If a partonic picture of the pomeron is used this implies that the forward hemisphere is like the forward hemisphere in e^+e^- annihilation.

Comparing with the data from the E.M.C. experiment it can be seen that there is no suppression in the H1 data of gluon radiation (the cause of the high x_F tail in the E.M.C. data) in the backward hemisphere, this suggests that the remnant from the interaction is not an extended object.

The plot of $< p_T^{*2} >$ vs x_F or the seagull plot is shown in fig. 5. The H1 data are compared with the result of E.M.C. and a prediction from RAPGAP. It can be seen that the $< p_T^{*2} >$ in the H1 data sits somewhat above that from the E.M.C. in both hemispheres, even though the average centre-of-mass energy in H1 is slightly below that of the E.M.C.. This suggests that a high proportion of events have a high p_T hard subprocess. The H1 seagull plot is also quite symmetric about $x_F = 0.$, showing that there is no suppression of gluon radiation in the backward hemisphere.

High Q^2 Di–Jet Production

In and fig. 6 we show the distribution of η_{max} for diffractive di-jet events. Also shown is a comparison with Monte Carlo simulations, where LEPTO6.1 [3] was used to describe the overall features of DIS events and RAPGAP2.02 for a description of diffractive events. The absolute normalisation of RAPGAP was taken from a QCD analysis of $F_2^{D(3)}$ and the relative normalisation of LEPTO was chosen such that the high η_{max} spectrum for the inclusive DIS sample is properly described. In fig. 7 the correlation and resolution in $\xi_{I\!P}$ is shown as obtained from a detailed simulation with the RAPGAP2.02 Monte Carlo. Using the Monte Carlo to correct to the hadron level, we obtain the di-jet cross section as a function of $\xi_{I\!P}$ as shown in fig. 8. The binning is chosen such that the purity is everywhere above 50%.

In fig. 9 the correlation and resolution in p_T of the two jets in the $\gamma^* I\!P$ centre-of-mass system is shown and is compared with a detailed simulation given by the RAPGAP2.02 Monte Carlo. Using the Monte Carlo to correct to the hadron level, we obtain the di-jet cross section as a function of p_T as shown in fig. 10. Note that here we have two entries per event, corresponding to each of the two jets. Both cross sections $\frac{d\sigma}{d\xi_{I\!P}}$ and $\frac{d\sigma}{dp_T}$ agree reasonably well with the predictions from the RAPGAP2.02 Monte Carlo, using a factorisable pomeron and a parametrisation of the parton densities of the pomeron from a QCD analysis of $F_2^{D(3)}$ [1]. The high Q^2 di-jet cross section comes from a contribution from QCD-Compton and BGF processes. Since the quark densities are constrained from $F_2^{D(3)}$ the QCD-Compton contribution can be evaluated. However the reasonable agreement of the Monte Carlo simulation with the data indicates that the gluon density in the pomeron can also be constrained.

Low Q^2 Di–Jet Production

In photoproduction the jet finding is carried out in the laboratory frame using a η_{lab} range of $-2.5 < \eta_{lab} < 3.5$ and $E_{t,jet} \geq 5$ GeV. It is possible to perform the analysis in the laboratory frame since there is no transverse boost associated with real photons. After a final jet cut of $-1.5 < \eta_{jet} < 2.5$ the cross sections are corrected to the hadron level for

$x_{\mathbb{P}} < 0.05$. In fig. 11 is shown the cross section for di-jet production in photoproduction as a function of x_γ ($d\sigma/dx_\gamma$) and in fig. 12 $d\sigma/dz$ together with a comparison with expectations from the POMPYT Monte Carlo, using different parametrisations of the parton densities in the pomeron. It can be seen that the shape of $d\sigma/dx_\gamma$ does not depend on the parametrisation of the parton densities in the pomeron, whereas the shape of the cross section as a function of z agrees well with a hard parton density of the form $\sim \xi(1-z)$ but not with a soft parton density $\sim (1-z)^5$. Note that here only shape comparisons are made since the parton densities used are not absolutely normalised. Note also that the POMPYT Monte Carlo does not have QCD evolution included.

Conclusion

Energy flows, charged particle spectra and jet cross sections have been measured in deep-inelastic diffractive scattering. The data show that there is a large contribution from high p_T events to the total cross section. The diffractive final state is also seen to be symmetric about $\eta^* \approx 0$ with no evidence of an extended remnant.

The differential cross sections of high Q^2 diffractive di-jet production are in reasonable agreement with a prediction from a factorisable pomeron with a parton density in which a leading gluon arises from a QCD analysis of $F_2^D(3)$. The data do not favour a solution in which only quarks are used at a starting scale of perturbative evolution of $2.5\,\mathrm{GeV}^2$.

In photoproduction the cross section as a function of z is sensitive to the parton density in the pomeron. A hard parton density of the form $\sim z(1-z)$ is consistent with the measurement but not a soft parton density $\sim (1-z)^5$.

Acknowledgments

We are grateful to the HERA machine group whose outstanding efforts have made and continue to make this experiment possible. We thank the engineers and technicians for their work in constructing and now maintaining the H1 detector, our funding agencies for financial support, the DESY technical staff for continual assistance, and the DESY directorate for the hospitality which they extend to the non-DESY members of the collaboration.

References

[1] H1 collaboration: *A Measurement and QCD Analysis of the Diffractive Structure Function* $F_2^{D(3)}$, paper pa02-061 contributed to this conference.

[2] A.Mehta, "Deep–Inelastic Diffraction", proceedings of Topical Conference on Hard Diffractive Processes, February 18-23 1996, Eilat, Israel.

[3] G. Ingelman, Proceedings of the Workshop on Physics at Hera, vol. 3, eds. W. Buchmüller, G. Ingelman, DESY (1992) p.1366.

[4] H1 Collaboration, The H1 Detector at HERA, DESY report 93-103, To be submitted to Nuclear Instruments and Methods.

[5] G. Ingelman and P. Schlein, Phys. Lett. **B152** (1985) 256.

[6] H. Lotter, J. Bartels, M. Wuesthoff, Quark-Antiquark Production in DIS Diffractive Dissociation, *DESY 96-026 hep-ph/9602363*
H. Lotter, C. Ewerez, J. Bartels, M. Wuesthoff, Azimuthal Distribution of Quark - Antiquark Jets in DIS Diffractive Dissociation, *DESY 96-085 hep-ph/9605356*
M. Wuesthoff, Photon Diffractive Dissociation in Deep Inelastic Scattering, *DESY 95-166*
M. Diehl, Diffractive Production of di-jets at HERA, *DAMTP-94-60 hep-ph-9407399* and contributions to workshop Future Physics at HERA, 1996, to be published

[7] H. Jung, *Hard diffractive scattering in high energy ep collisions and the Monte Carlo generator RAPGAP Comp. Phys. Comm.* 86 (1995) 147
H. Jung *RAPGAP2.02 Program Manual* 1996 unpublished

[8] P. Bruni and G. Ingelman, *Diffractive Hard Scattering at ep and $p\bar{p}$ Colliders*, DESY 93-187 (1993) and in: J. Carr and M. Perrottet (editors) *Proceedings of the International Europhysics Conference on High Energy Physics* p.595-596, Marseilles 1993.

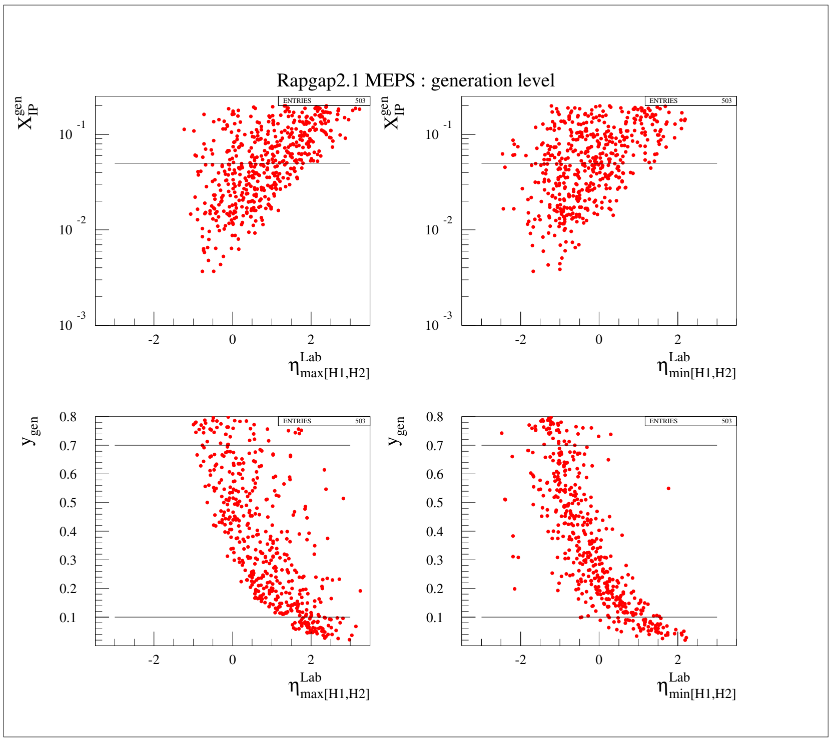

Figure 1: Correlation of η_{jet} with the kinematic variables y and $x_{\mathbb{P}}$. The lines indicate the final cuts used for the high Q^2 sample of diffractive di - jets.

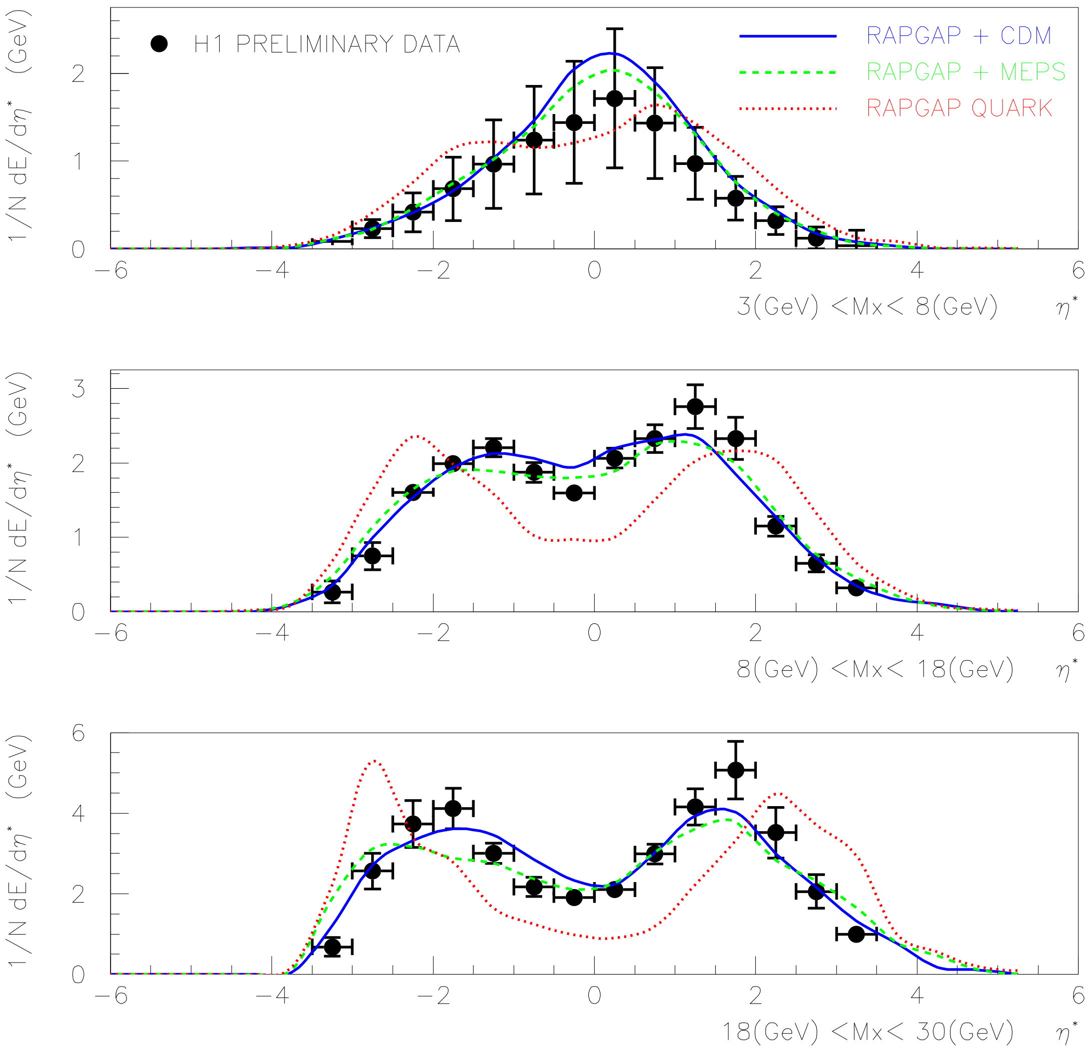

Figure 2: Energy-flows as a function of M_X fully corrected H1 data compared with predictions from RAPGAP. The γ^* points in the positive direction of pseudo-rapidity.

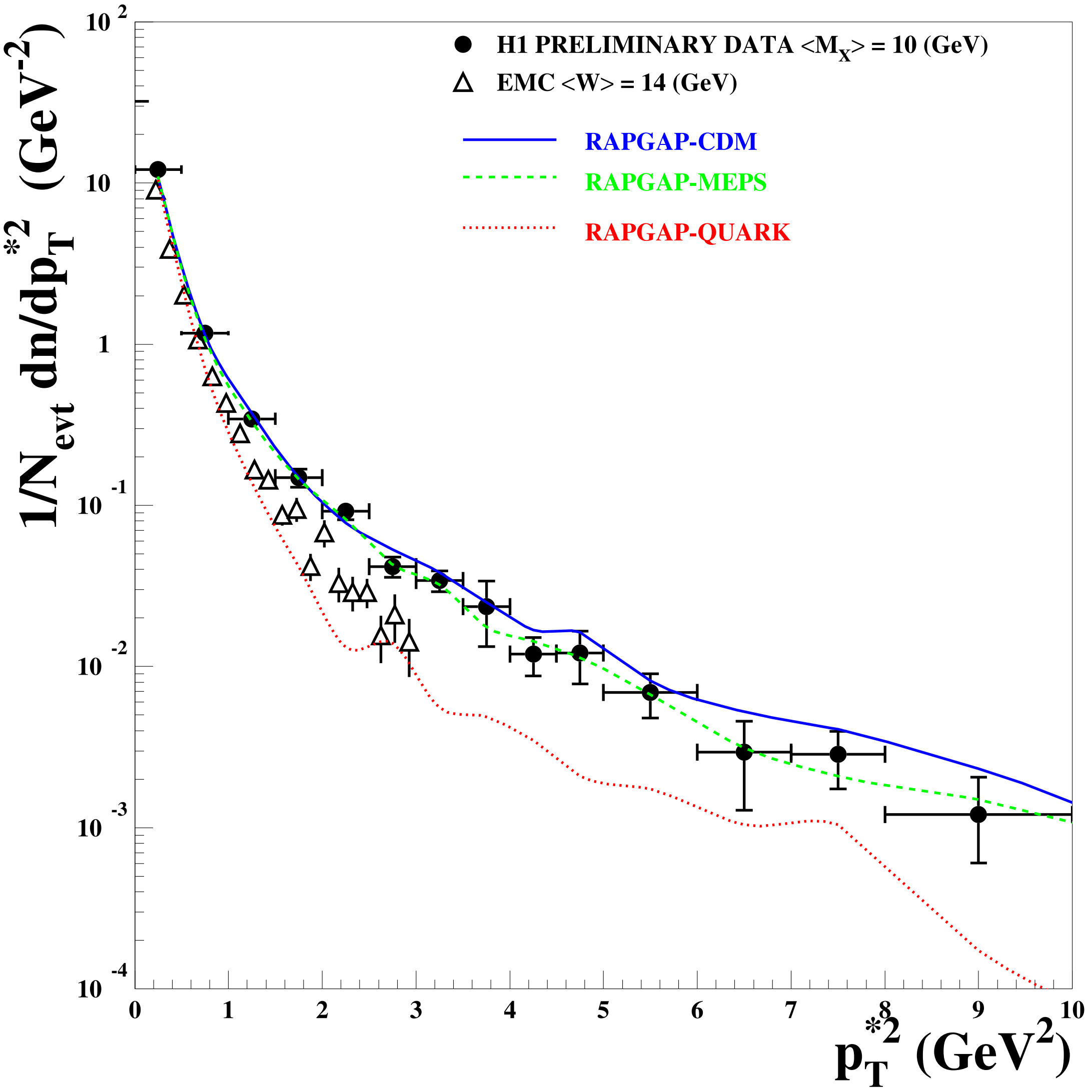

Figure 3: p_T^{*2} plot showing fully corrected H1 data compared with E.M.C. data at higher energy and predictions from RAPGAP.

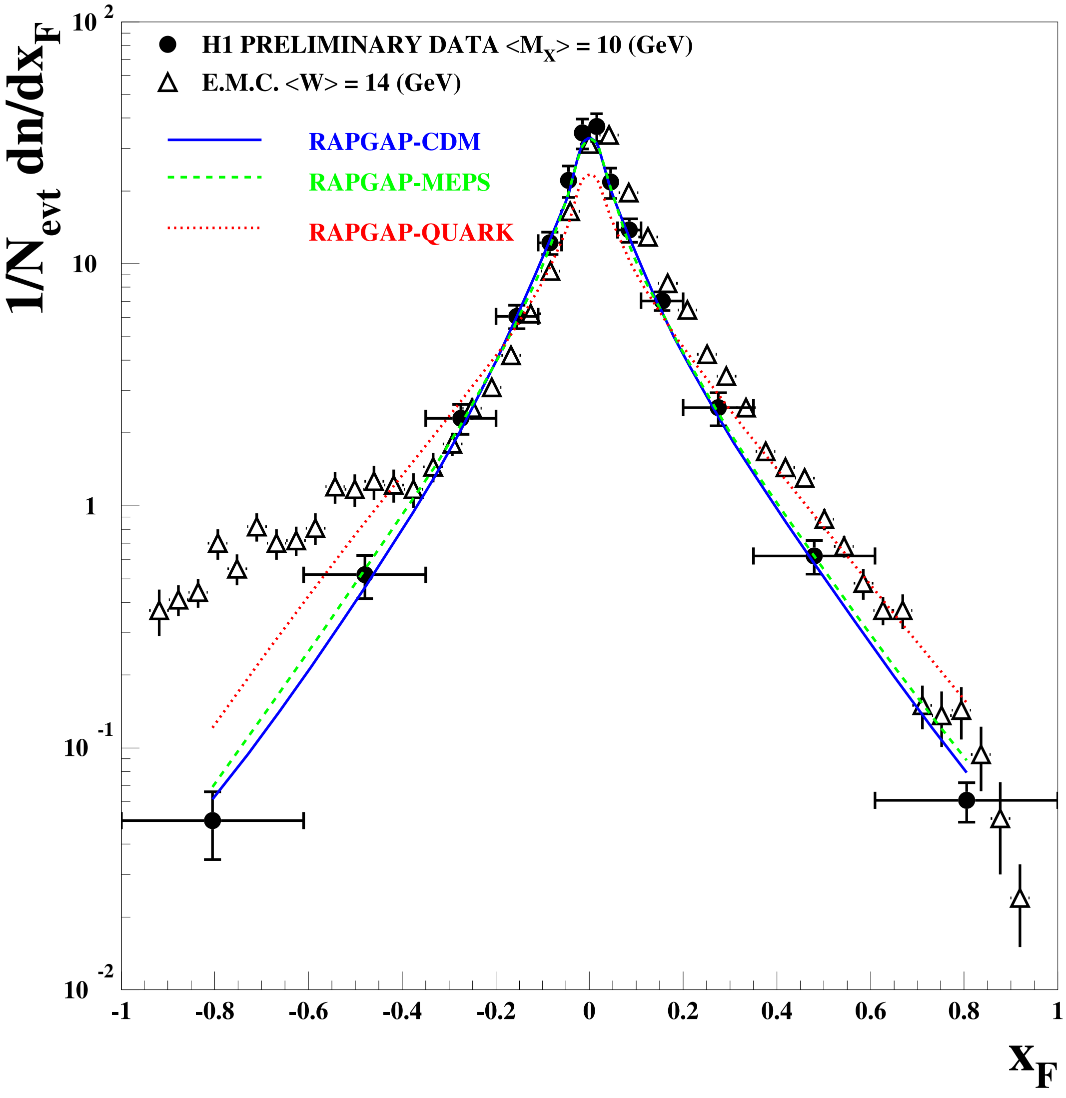

Figure 4: x_F plot showing fully corrected H1 data compared with E.M.C. data at higher energy and predictions from RAPGAP.

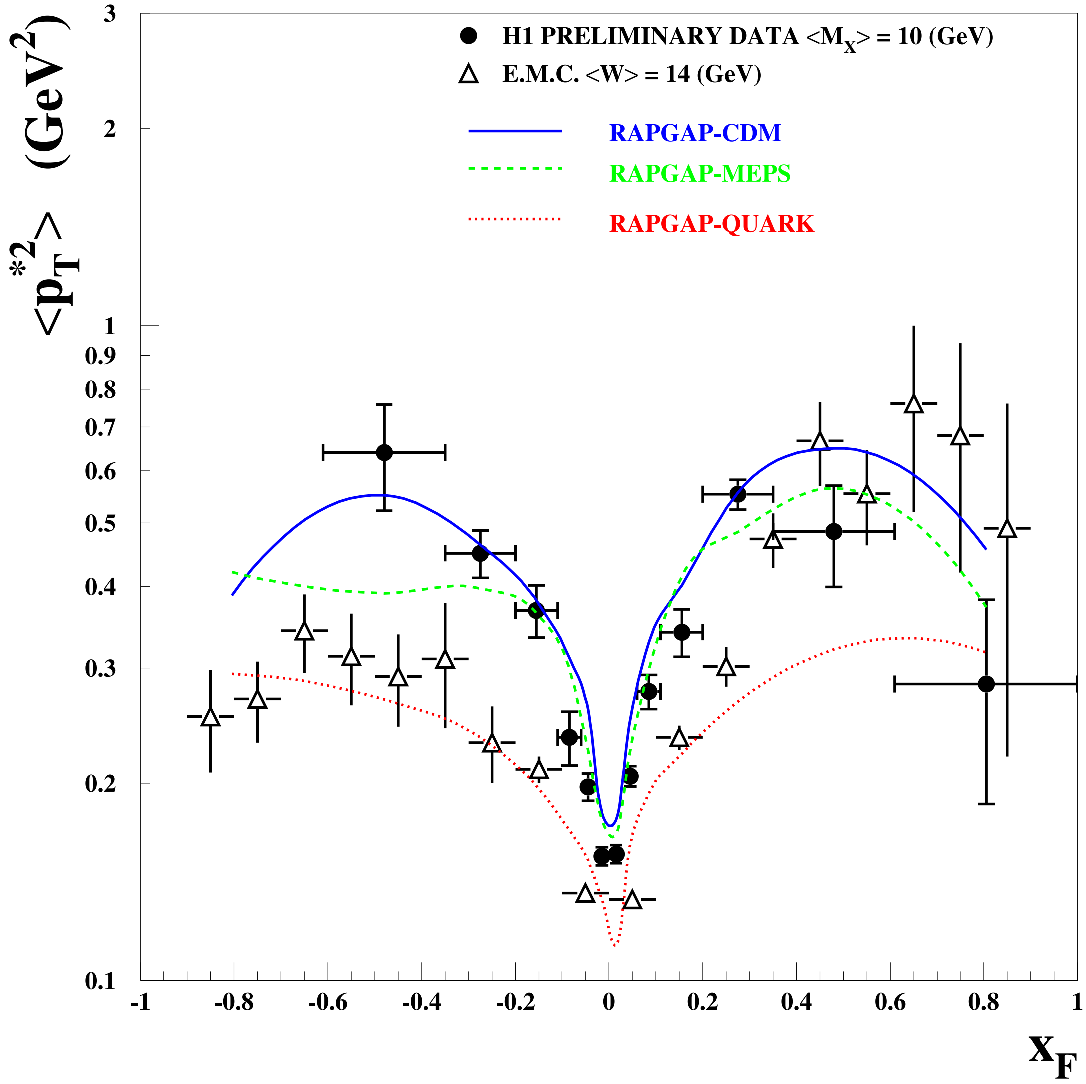

Figure 5: Seagull plot showing fully corrected H1 data compared with E.M.C. data at higher energy and predictions from RAPGAP.

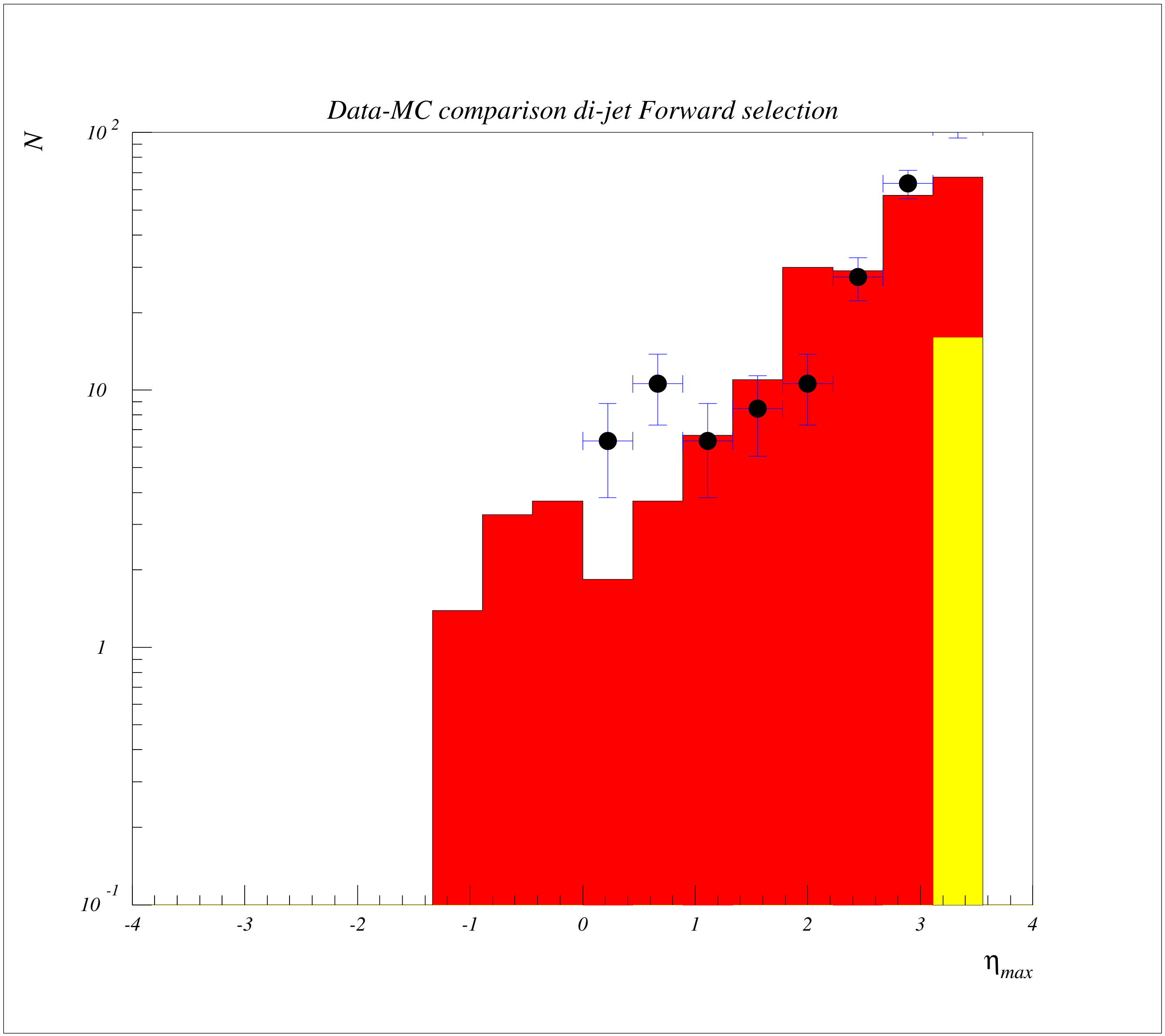

Figure 6: η_{max} distribution the high Q^2 diffractive di-jet events sample. The light shading is the contribution from standard DIS and the dark shading the contribution from diffractive DIS. The data are the black points.

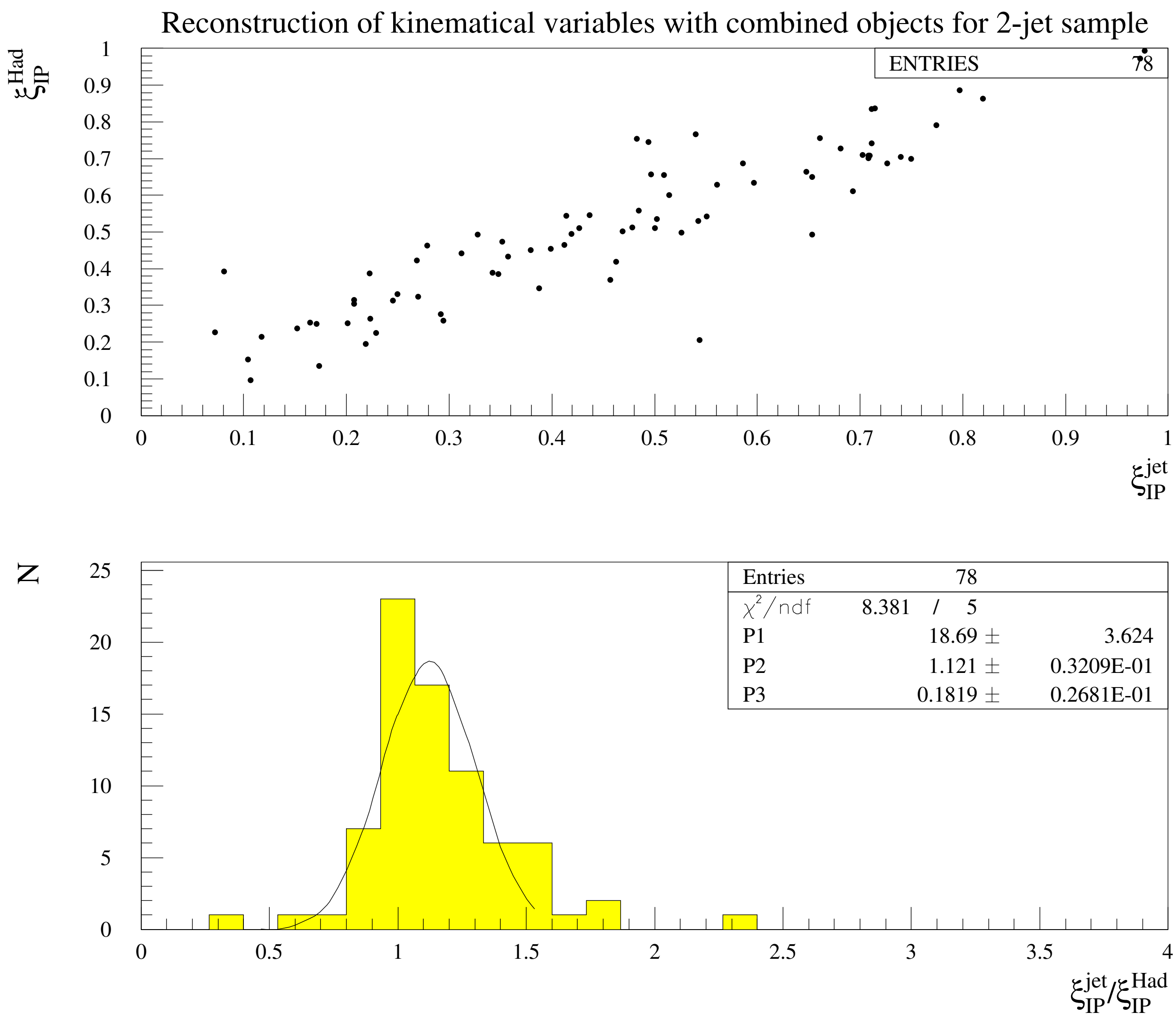

Figure 7: Correlation of $\xi_{I\!P}$ at the hadron level with $\xi_{I\!P}$ reconstructed, and the resolution in $\xi_{I\!P}$ obtained from a simulation with RAPGAP.

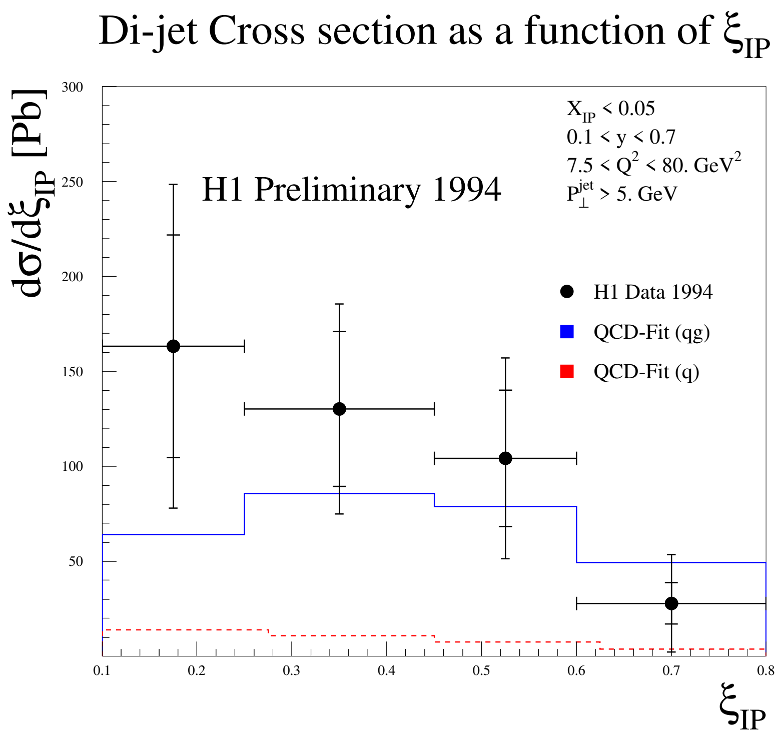

Figure 8: Cross section $\frac{d\sigma}{d\xi_{I\!P}}$ for the high Q^2 sample within $0.1 < y < 0.7$, $7.5 < Q^2 < 80$ $x_{I\!P} < 0.05$ and $p_T > 5$. The inner error bar on the data are statistical errors only, the full error bars are statistical and systematic errors added in quadrature. Shown in the solid line, the prediction from RAPGAP using parton densities obtained from the QCD analysis of $F_2^{D(3)}$. Also shown in the dashed line is the prediction from RAPGAP in which the parton densities are constrained to be quarks at the starting scale.

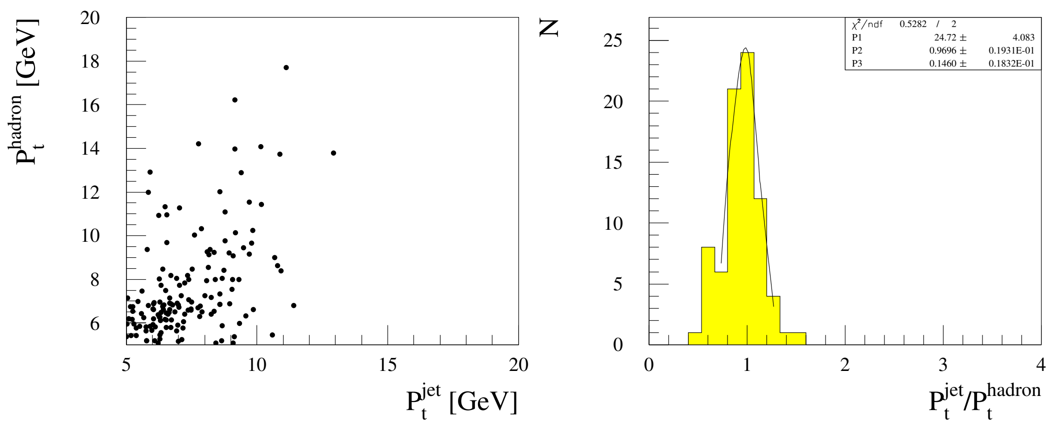

Figure 9: Correlation of p_T at the hadron and the reconstructed level as obtained from a Monte Carlo simulation.

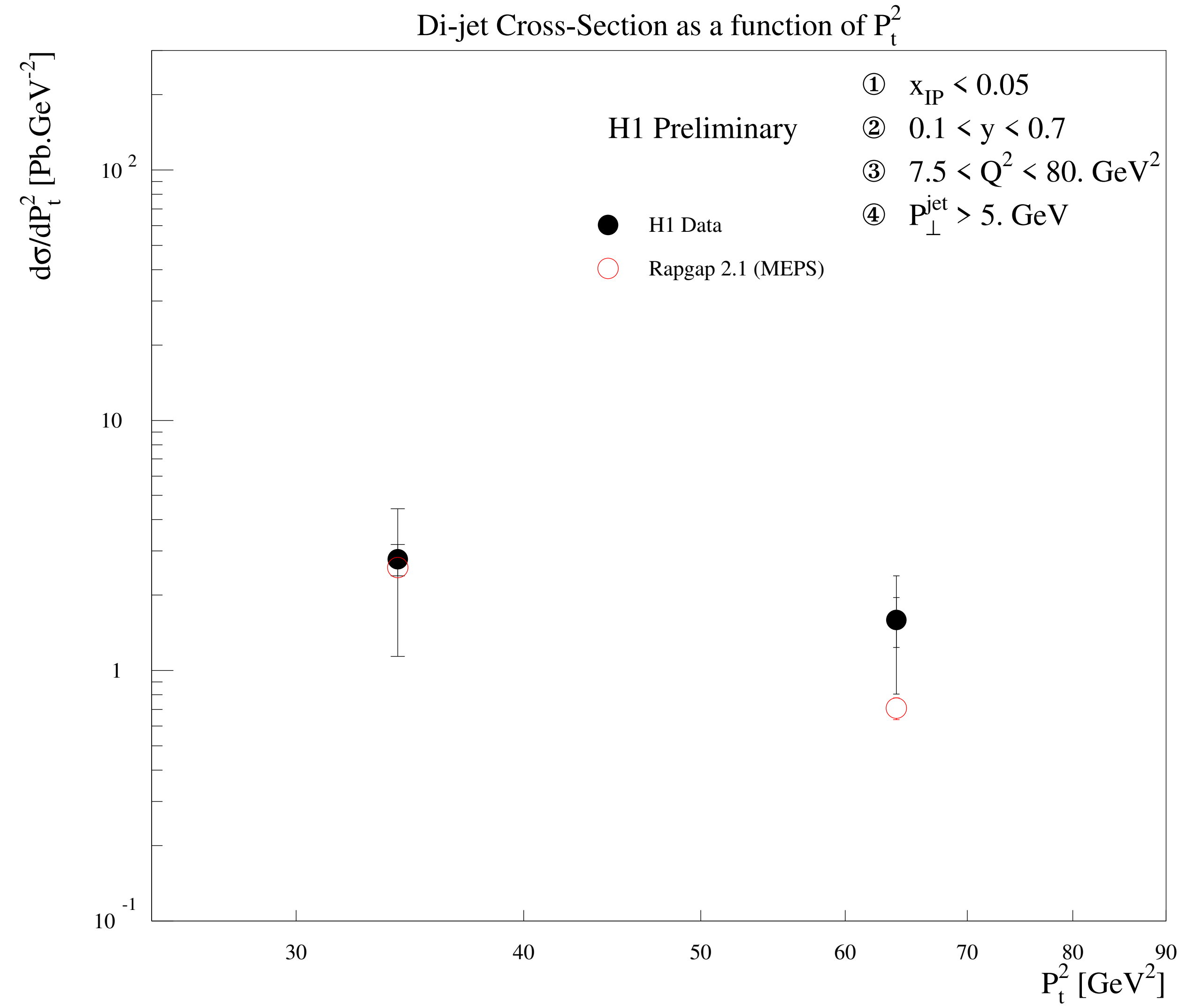

Figure 10: Cross section $\frac{d\sigma}{dp_\perp}$ for the high Q^2 sample within $0.1 < y < 0.7$, $7.5 < Q^2 < 80\,\mathrm{GeV}^2$ $x_{\mathbb{P}} < 0.05$ and $p_T > 5$. The inner error bar on the data are statistical errors only, the full error bars are statistical and systematic errors added in quadrature. Also shown is the prediction from RAPGAP using parton densities obtained from the QCD analysis of $F_2^{D(3)}$. The errors on the Monte Carlo are statistical only.

H1 preliminary 1994

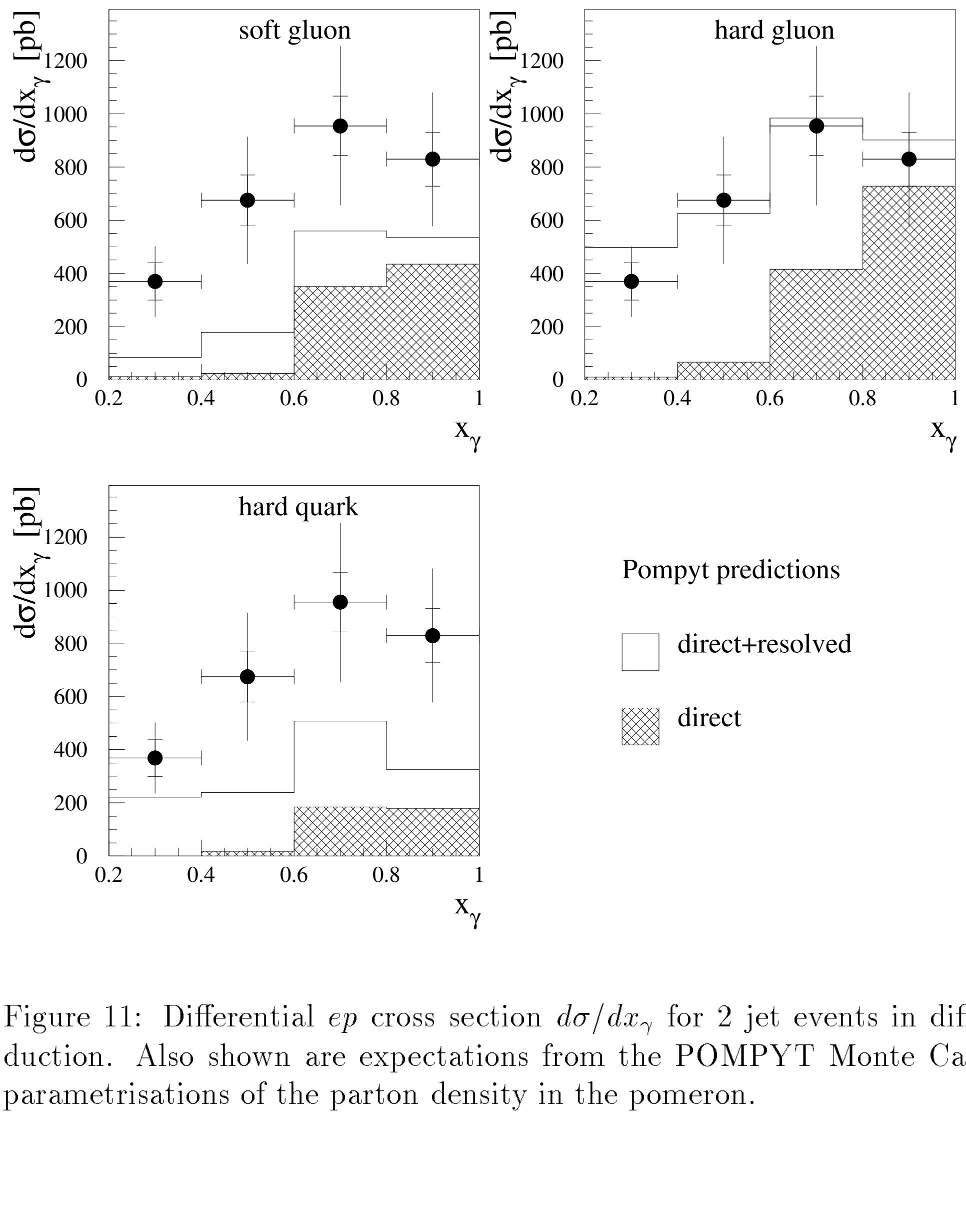

Figure 11: Differential ep cross section $d\sigma/dx_\gamma$ for 2 jet events in diffractive photoproduction. Also shown are expectations from the POMPYT Monte Carlo using different parametrisations of the parton density in the pomeron.

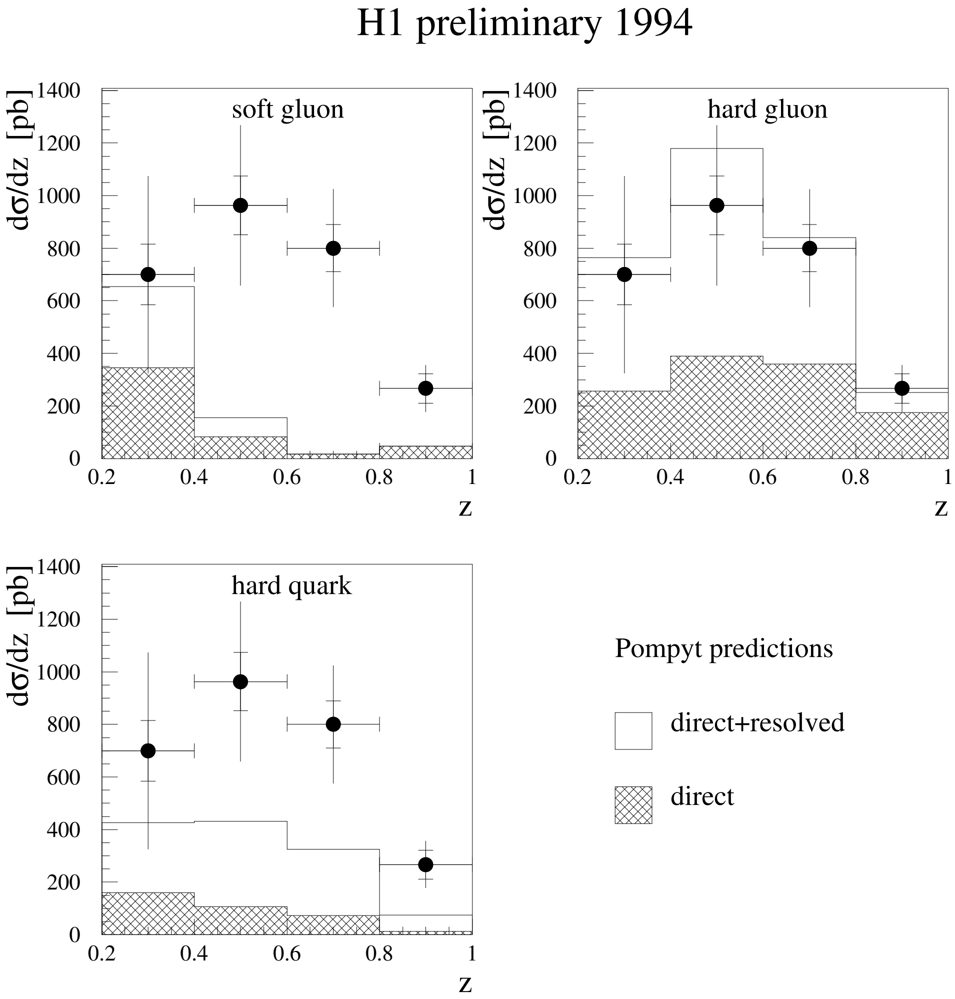

Figure 12: Differential ep cross section $d\sigma/dz$ for 2 jet events in diffractive photoproduction. Also shown are expectations from the POMPYT Monte Carlo using different parametrisations of the parton density in the pomeron.